The effect of fuel composition and temperature on the interaction of H_2S with nickel–ceria anodes for Solid Oxide Fuel Cells

P. Lohsoontorn [a], D.J.L. Brett [b], N.P. Brandon [a,*]

[a] Department of Earth Science and Engineering, Imperial College London, London SW7 2AZ, United Kingdom
[b] Department of Chemical Engineering, University College London, London WC1E 7JE, United Kingdom

ARTICLE INFO

ABSTRACT

The impact of H_2S on nickel–gadolinium-doped ceria (Ni–CGO) used as the anode for solid oxide fuel cells has been studied over a range of operating conditions using yttria-stabilised zirconia electrolytes. This included varying the partial pressure of H_2S and H_2 in the fuel mixture as well as the operating temperature. Electrochemical impedance measurements were made on symmetrical cells under each operating condition and compared with thermodynamic predictions of the state of the material as a function of operating condition. Increasing the H_2S concentration (1–3 ppm H_2S in moist H_2) significantly increased the anode degradation. A decrease in H_2 content in the fuel (97–9.7% H_2) was found to increase the degree of sulphur interaction with the anodes. Lowering the operating temperature (873–830 K) showed an increase in the detrimental impact of sulphur on the anode. This experimental result was compared to thermodynamic predictions, which show the dependency of Ni–S interaction on pS_2 and temperature as well as the effect of ceria–S interaction on pO_2 and pS_2. The consequence of this study shows that the interaction of sulphur with the anode is strongly dependent on gas composition and operating condition—suggesting that different parts of the anode can be degraded differently, stressing the importance of a well-designed gas flow field and temperature distribution management.

© 2008 Elsevier B.V. All rights reserved.

1. Introduction

The solid oxide fuel cell (SOFC) is a promising energy conversion technology due to its high efficiency, ability to deliver high-grade heat and electrical power, and because of its fuel flexibility. In contrast to low temperature fuel cells, such as the polymer electrolyte fuel cell (PEFC), the SOFC can operate on hydrocarbon fuel either directly or with a minimum of fuel processing, so reducing the cost of the system, maximizing efficiency and using readily available fuel as opposed to pure hydrogen. However, most hydrocarbon fuels contain a range of sulphur containing compounds [1–3], which often have a detrimental impact on anode performance and is one of the major challenges facing the implementation of fuel flexible SOFCs.

Sulphur removal is possible, and various solutions have been proposed [3–6]; however, obtaining ultra-low levels of sulphur in the fuel is difficult without resorting to bulky and potentially expensive desulphurisation units. Incorporation of a desulphurisation stage also complicates the whole fuel cell system in terms of thermal integration and the need for periodic sorbent/catalyst regeneration. In contrast to the removal of sulphur compounds before they reach the SOFC, alternative anode materials are being developed that are tolerant to sulphur in the fuel [7–22]. Alternatively, the combination of a desulphurization stage and sulphur-tolerant anodes may be used, which will relax the performance requirements of both aspects of the system.

In order to determine how much sulphur an SOFC anode can withstand and to inform materials selection for improved sulphur resistance, an understanding of the mechanism and factors that influence anode interaction with sulphur must be obtained. The literature shows that the interaction of sulphur with an SOFC anode relies significantly on the operating conditions [23–27]. Therefore, it is of interest to study the factors that influence the interaction of sulphur with the anode (e.g. gas compositions and operating temperature). The study has focused on low concentrations of sulphur (<10 ppm) to capture the range of sulphur concentrations that can be found in natural gas before and after a sulphur removal processes, including the concentration of sulphur that could remain in the fuel gas if the removal process has failed.

The aim of this study is to investigate the effect of pH_2S, pH_2 and operating temperature, on the interaction of (1–3 ppm) H_2S with nickel-based anode cermets used for intermediate temperature solid oxide fuel cells (IT-SOFCs).

* Corresponding author. Tel.: +44 20 75945704; fax: +44 20 75947444.
E-mail address: n.brandon@imperial.ac.uk (N.P. Brandon).

Electrochemical impedance measurements on symmetrical fuel cells was chosen as an appropriate means of gaining information on the change in electrochemical performance of the anodes when exposed to H_2S under various operating conditions. This technique allows for the delineation of the various losses in the anode and is not complicated by the performance of the cathode. The limitation is that the performance of the anode can only be studied at open circuit. Further work is currently being performed using a three-electrode arrangement which is providing information on the effect of H_2S on anodes subject to a net flux of O^{2-}.

To help rationalize the experimental results, phase equilibrium diagrams of Ni and ceria across a range of S_2 and O_2 compositions were obtained from thermodynamic calculations.

2. Experimental

2.1. Cermet symmetrical cell fabrication

Cermet symmetrical cells of nickel–gadolinium-doped ceria deposited on both sides of yttria-stabilised zirconia (Ni–CGO/YSZ/Ni–CGO) were fabricated. Yttria-stabilised zirconia (YSZ) was chosen as the electrolyte material in place of CGO (gadolinium-doped ceria) in order to avoid experimental artefacts arising from the mixed ionic/electronic conductivity (MIEC) exhibited by CGO in low pO_2 environments at elevated temperatures; this has been found to make the impedance response much more complex and difficult to interpret [28]. YSZ powder (8 mole% Y_2O_3, Tosoh, Japan) was uniaxially pressed (1 tonne, 30 s), followed by sintering at 1723 K in air for 5 h—giving a dense pellet (~95% calculated density) with a diameter of ~11.9 mm and thickness of ~1.27 mm. The NiO–CGO layers, giving the ratio of Ni to CGO after reduction of 50 wt.% $Ce_{0.9}Gd_{0.1}O_{1.95}$ and 50 equiv. wt.% Ni (NextTech Materials, USA), were deposited on both sides of the dense electrolyte and

fired at 1573 K for 2 h. The reduction of NiO to Ni was performed in 97% H_2/3% H_2O for 1 h at the experimental temperature (873 K or 830 K). This resulted in a cermet layer with a thickness of ~100 μm.

2.2. Electrochemical impedance analysis

Electrochemical impedance spectroscopy (EIS) was performed using an Autolab PGSTAT30 fitted with a frequency response analyser (FRA) (Autolab, EcoChemie, Netherlands). The instrumentation was controlled using FRA for Windows (version 4.9.004) which allowed fitting of the complex plane impedance data to equivalent circuit models. The non-linear least squares fit was performed using the approach of Boukamp [29]. Impedance measurements were performed in potentiostatic mode using a sinusoidal signal amplitude of 20 mV$_{rms}$ over the frequency range of 10 kHz to 10 mHz. Fig. 1(a) shows the head of the test rig used for the impedance measurement. Electrical connection was made to the electrodes of the symmetrical cells via platinum wires connected to a fine platinum mesh (mesh 99.99% Pt, 0.06 mm wire diameter, 0.25 mm aperture; wire 99.99% Pt, 0.25 mm diameter, both GoodFellow, UK) and put into compression using the two tie rods (Inconel) shown with springs in tension outside of the furnace hot zone. The cell holder was then placed inside a quartz tube, with gas inlet and outlet points, so allowing the gaseous environment exposed to the cell to be controlled. A tube furnace (Lenton, UK) was used to control the temperature of the rig.

The electrochemical impedance response was fitted to an equivalent circuit composed of a resistor in series with two parallel constant phase element (CPE)/resistor combinations, shown in Fig. 1(c). The CPE is used, as opposed to a pure capacitance, due to the finite thickness of the porous electrode having a distributed electrochemical response that results in the centre of circular arc being suppressed below the horizontal axis on the complex plane
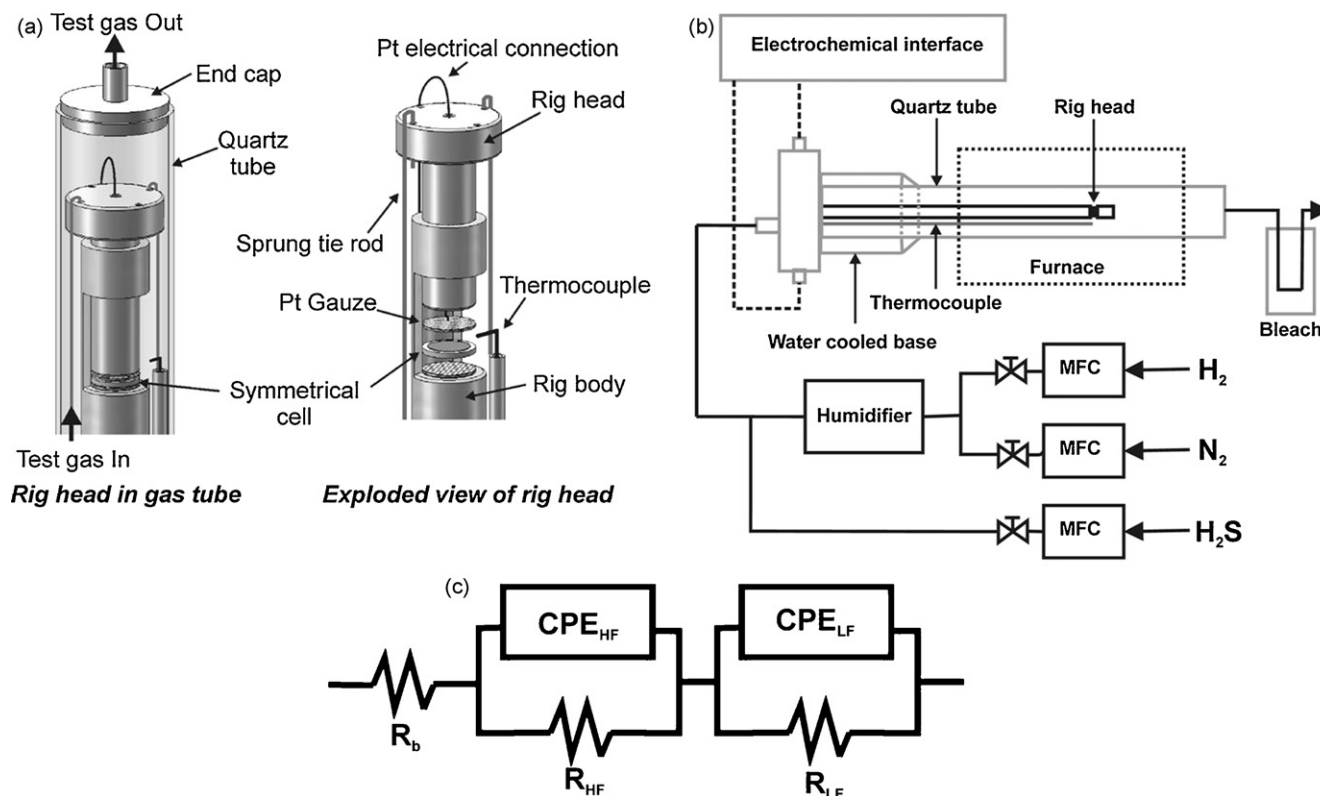

Fig. 1. Test system: (a) head of test rig for electrochemical impedance measurement; (b) test system; (c) an equivalent circuit for impedance response fitting.

Table 1
Calculated errors from equivalent circuit fitting using the non-linear least squares method

Operating condition	Fitting error (%)		
	HF-intercept	HF arc	LF arc
97% H_2, 3% H_2O, 873 K	0.01–0.02	1.2–2.1	1.4–7.9
97% H_2, 3% H_2O, 1 ppm H_2S, 873 K	0.01–0.02	1.1–4.9	1.7–7.7
97% H_2, 3% H_2O, 3 ppm H_2S, 873 K	0.02–0.03	1.5–3.1	1.4–8.8
48.5% H_2, 3% H_2O, 1 ppm H_2S, 873 K	0.02–0.03	1.0–1.8	0.7–3.4
9.7% H_2, 3% H_2O, 1 ppm H_2S, 873 K	0.03–0.04	1.0–5.3	2.1–4.0
97% H_2, 3% H_2O, 1 ppm H_2S, 830 K	0.01–0.02	1.5–6.2	4.2–6.8

diagram [30,31]. The estimated error from the least squares fitting ranges from 0.01 to 8.8%, depending on impedance components and experimental conditions. The calculated error under various experimental conditions is shown in Table 1. Since a symmetrical cell is used, the impedance values obtained were halved to get the value per electrode.

The anode symmetrical samples were exposed to varied H_2S concentrations from 1 to 3 ppm (under constant conditions of 97% H_2, 3% H_2O, and 873 K). The effect of H_2 concentration was investigated by varying pH_2 between 97 and 9.7% H_2 under constant conditions of 1 ppm H_2S, 3% H_2O (N_2 balance) at 873 K. The operating temperature was varied from 830 to 873 K at constant fuel conditions of 1 ppm H_2S, 97% H_2 and 3% H_2O.

Fig. 1(b) shows the experimental set-up for the delivery of gas to the samples in the furnace. The test system allows different compositions of H_2S, H_2, N_2, and H_2O to be introduced to the cell. The H_2 and N_2 gas lines (both 99.99%, BOC, UK) connect to calibrated mass flow controllers (Bronkhorst, UK) which are available for gas flow rates ranging from 20 to 1000 cm^{-3} min^{-1}. After passing through the mass flow controllers, the H_2/N_2 line passes through the humidifier, which is a bubble column situated inside a thermocirculator bath, to saturate the gas with water. The H_2S is introduced from a stock bottle of 10 ppm H_2S in H_2 (certificated ±5% mixture accuracy, BOC, UK) which passes through a calibrated mass flow controller, that is available for gas flow rates ranging from 4 to 100 cm^{-3} min^{-1}, and is combined with the humidified stream to give the requisite gas composition in the heated chamber. Nylon tubing is used to minimise interaction of H_2S with steel tubing. Gas exiting the rig was scrubbed of H_2S by bubbling through a column of sodium hypochlorite.

3. Results and discussion

3.1. EIS measurements

3.1.1. The base response in H_2S-free atmosphere

EIS measurements were initially performed on Ni–CGO cermet symmetrical cells (Ni–CGO/YSZ/Ni–CGO) in an H_2S-free atmosphere to establish the base response expected from the cell when not being affected by a sulphur containing fuel stream. Fig. 2 shows that the generic form of the impedance response is composed of two partially resolved arcs. To help determine the origin of these features, the gas composition and temperature were varied to see how these factors influence the response. Fig. 2(a) shows how the EIS response varied for H_2 concentrations ranging from 9.7 to 97% (constant 3% H_2O, N_2 balance) at a constant temperature of 873 K, and Fig. 2(b) shows the response when the temperature was varied from 833 to 873 K at constant H_2 content (97% H_2, 3% H_2O). At constant temperature, the low frequency arc (LF arc) varied significantly with H_2 content (decreasing with increasing pH_2), while the high frequency arc (HF arc) remained unaffected, as can be seen inset in Fig. 2(a). This contrasts with the response when the tem-
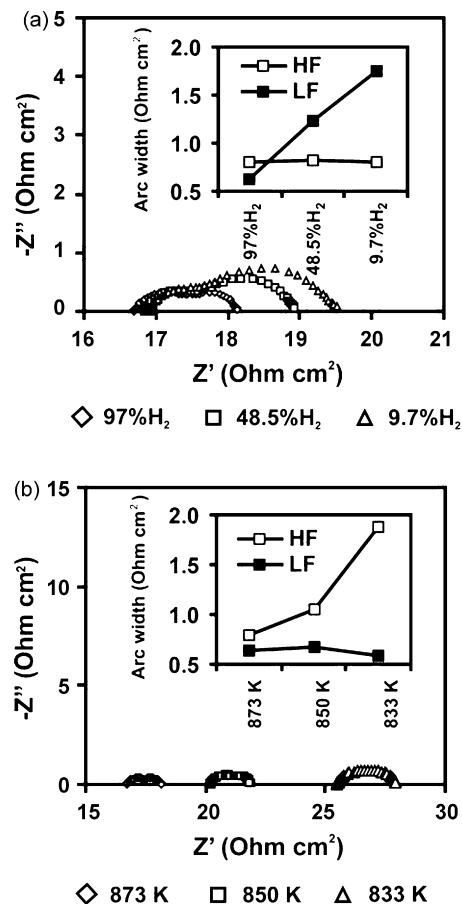

Fig. 2. Electrochemical impedance measurements on symmetrical cells (Ni–CGO/YSZ/Ni–CGO) exposed to varying operating conditions: (a) varied H_2 content from 97 to 9.7% at a constant temperature of 873 K (3% H_2O), the figure inset shows the HF and LF arc width, plotted with H_2 content; (b) impedance response at varied temperature from 838 to 873 K at a constant H_2 content (97%, 3% H_2O), the figure inset shows the HF and LF arc width plotted with temperature.

perature was varied while maintaining a constant H_2 concentration of 97%, as shown in Fig. 2(b) and inset. At constant pH_2, the HF arc increased significantly with decreasing temperature while the LF arc remained effectively constant. This suggests that the HF arc can be considered a manifestation of the charge transfer resistance, while the LF arc can be reasonably attributed to mass transport effects. The shift in the position of the arc along the real-axis (Z'), associated with operation at different temperatures, is due to a change in the purely ohmic response of the cell which is a consequence of the change in ionic conductivity of the YSZ pellet with temperature.

Fig. 3 shows how the impedance response develops with time when a Ni–CGO symmetrical cell is exposed to a sulphur-free atmosphere (97% H_2 and 3% H_2O) at 873 K for 60 h. The impedance spectra were fitted to the equivalent circuit using a non-linear least squares method, as mentioned previously. The fitting values were plotted separately as the HF, LF, and total arc width, as well as the high frequency intercept of the impedance arc with the real-axis (HF intercept). The total impedance plot shows that the cell performance degrades monotonically with time. Also, it can be seen that an increase in the total arc impedance was entirely due to an increase in the HF feature, while the LF feature remained comparatively stable. Although the total impedance arc width showed a non-linear trend, a linear approximation over the entire 60 h period gave a base degradation rate of 0.03 Ω cm^2 h^{-1}, for the half cell in
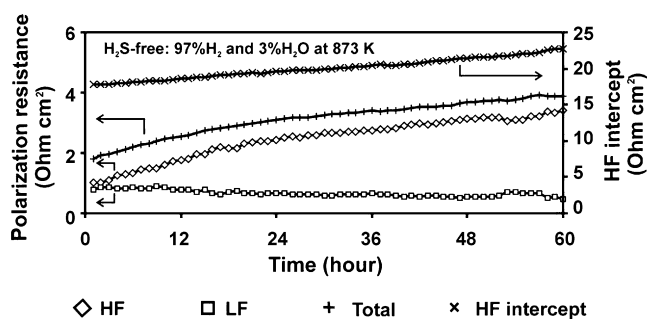
Fig. 3. The plot of impedance response of the Ni–CGO half cell (Ni–CGO/YSZ/Ni–CGO) exposed to 97% H_2 and 3% H_2O at 873 K for 60 h. The plot shows the HF real-axis intercept, HF feature, LF feature, and total arc width of the impedance spectra in H_2S-free atmosphere.

a H_2S-free atmosphere, with the HF intercept exhibiting a linear resistance increases at a rate of $0.08\,\Omega\,cm^2\,h^{-1}$.

The response observed without the presence of sulphur is the inherent degradation of the anode. It is clear that this needs to be improved and is an indication that the electrode material has been optimized for performance but not durability. Anode performance loss under steady state conditions can be caused by a number of factors; Ni sintering resulting in loss of active surface area and reduced conductivity of the anode is one of the major causes [26].

3.1.2. Effect of pH_2S on the interaction between H_2S and Ni–CGO anodes

Fig. 4 shows the changes in the impedance spectra of a Ni–CGO cermet symmetrical cell when exposed to a varied H_2S concentration (1 and 3 ppm H_2S) at 867 K in a constant concentration of hydrogen and steam (97% H_2, 3% H_2O). Each cell was initially exposed to a H_2S-free atmosphere (97% H_2, 3% H_2O) for 12 h to establish the base line of the degradation rate before H_2S was added for 24 h. To study the recovery of the half cell, the H_2S source was removed and the cell returned to the same conditions as prior to H_2S exposure. Considering the impedance spectra shown in Fig. 4(a) and (b), increasing pH_2S significantly increased both the rate and extent of cell performance degradation.

To see how the features of the impedance response develop with time for the two H_2S concentrations, the anode polarization resistance (total arc width) is plotted in Fig. 4(c). Considering the total anode polarization resistance, the degradation profile with time can be divided into two steps: an initial 'rapid' increase in resistance over the course of a few hours, followed by a relatively slow performance loss. Other work has reported similar behavior [32–34]. Sasaki et al. [32] reported that the initial degradation may be caused by surface phenomena (e.g. the dissociative adsorption of sulphur species around the three phase boundary) while the second stage of degradation was attributed to the oxidation of Ni to NiO caused by the voltage drop associated with sulphur poisoning when operated in galvanostatic mode. Mukerjee et al. [33] and Ishikura et al. [34] both attribute an initial loss in performance to the adsorption of sulphur species on the actives sites; however, Ishikura et al. propose that the second step of degradation is the result of nickel sulphide diffusion into the anode/electrolyte layer. However, it should be noted that the work of Ishikura et al. was performed at 1173 K, above both the melting point of nickel sulphide and the temperatures used in this study. Increasing pH_2S significantly increased both the rate and degree of the total cell polarization resistance. The base case (H_2S-free) is also plotted for reference. The 'rapid' degradation step in 1 ppm H_2S took ~5 h ($0.26\,\Omega\,cm^2\,h^{-1}$) to reach the transition point to the 'slow' degra-
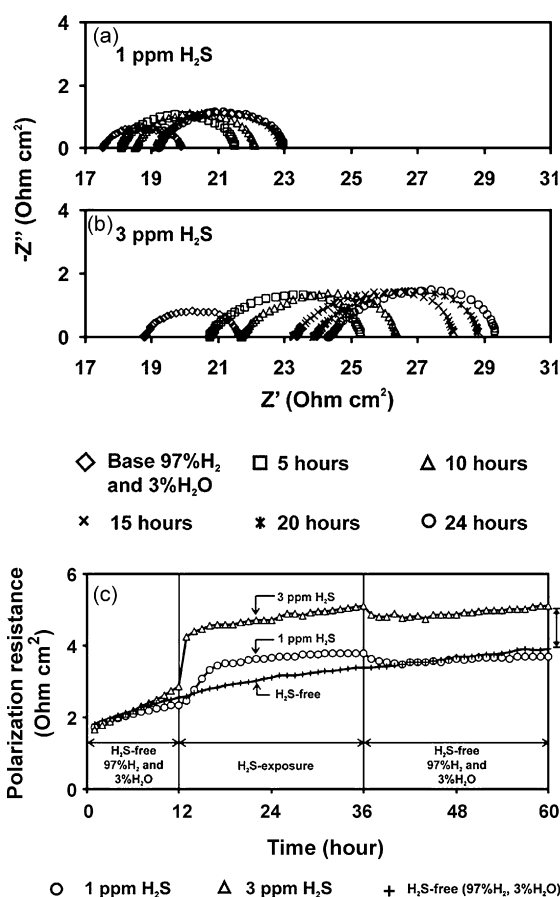

Fig. 4. EIS response of Ni–CGO half cell (Ni–CGO/YSZ/Ni–CGO) exposed to varied H_2S concentration: (a) 1 ppm H_2S; (b) 3 ppm H_2S, all at constant H_2, H_2O content and temperature (97% H_2, 3% H_2O, and 867 K); (c) total polarization resistance obtained from equivalent circuit fitting.

dation regime, while it was only ~2 h ($0.78\,\Omega\,cm^2\,h^{-1}$) for that in 3 ppm H_2S. The extent of the polarization impedance increase for 3 ppm H_2S exposure ($\Delta R_{polarization} = 4.8\,\Omega\,cm^2$) was greater than that for 1 ppm H_2S exposure ($\Delta R_{polarization} = 1.4\,\Omega\,cm^2$).

After H_2S exposure for 24 h, the sulphur source was removed and the cells were left in humidified H_2 (97% H_2, 3% H_2O) for 24 h. Compared to the cell running H_2S-free for 60 h, the cell exposed to 1 ppm H_2S was able to fully recover, while the cell exposed to 3 ppm H_2S could only be partially recovered, compared to the base case.

It can be seen in Fig. 4(a) and (b) that there is a shift in the high frequency intercept with the real-axis upon introduction of H_2S. This is more significant for the 3 ppm case, the 1 ppm exposure not being discernibly greater than the background observed for H_2S-free operation. The increase in ohmic resistance observed here, has also been reported by Tomita et al. who attribute it to the reaction of sulphur with the Ni component of the cermet [17].

To deconvolute the contributions to the overall impedance response, the HF and LF features were fitted and plotted separately, as shown in Fig. 5. It was observed that for 1 ppm H_2S, the HF component of the impedance response increased while the LF component was unaffected. In contrast, addition of 3 ppm H_2S resulted in an increase in both the HF and LF component. This implies that the higher concentration of H_2S has an effect on both the charge transfer resistance and mass transport properties, while at 1 ppm H_2S only the resistance to charge transfer is affected.
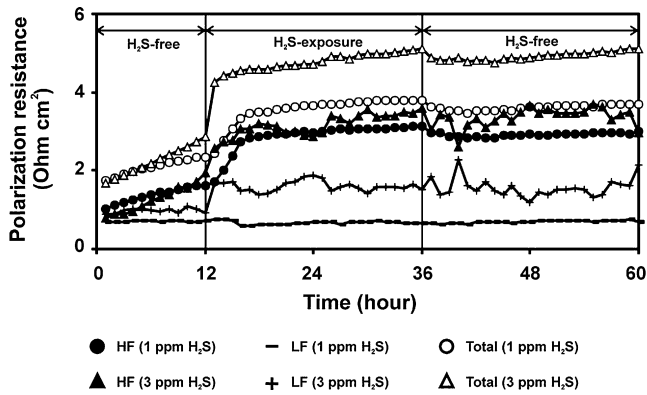
Fig. 5. High frequency, low frequency, and total EIS response when Ni–CGO half cells are exposed to 1 and 3 ppm H_2S in 97% H_2 and 3% H_2O at 873 K.

3.1.3. Effect of pH₂ on the interaction between H₂S and Ni–CGO anodes

Fig. 6(a)–(c) presents the EIS response when the Ni–CGO symmetrical cell was exposed to 1 ppm H_2S in varied concentrations of H_2 (97, 48.5, and 9.7%), while the pH_2O and temperature were maintained constant at 3% H_2O and 873 K. Fig. 6(d) shows the total anode polarization resistance plotted with time. Considering the base line (H_2S-free atmosphere in the first 12 h), the impedance of the cell in 9.7% H_2 (3% H_2O, N_2 balance) was higher than that at higher H_2 concentrations, mainly due to a larger mass transport effect. It was found that the detrimental effect of H_2S on the total polarization resistance of the cell was exaggerated by lowering the pH_2 level. The change in resistance at the end of the exposure time was measured to be: $\Delta R_{polarization}$ = 1.4, 3.7, and 13.6 Ω cm^2 for 97, 48.5, and 9.7% H_2, respectively. As mentioned previously, the 'rapid' degradation step in 1 ppm H_2S and 97% H_2 took ~5 h (0.26 Ω cm^2 h^{-1}) to reach the transition point to the 'slow' degradation regime. It was 12 h for the degradation in 48.5% H_2 (0.33 Ω cm^2 h^{-1}). For 9.7% H_2, the impedance response constantly increased over the exposure period of 1 ppm H_2S (0.49 Ω cm^2 h^{-1}).

As shown in Fig. 6(d), the degraded cell in 9.7% H_2 was not able to recover after removal of the sulphur source, and the half cell's performance continued to degrade (0.44 Ω cm^2 h^{-1}) at approximately the same rate as that with the H_2S present. The cell exposed to 1 ppm H_2S in 48.5% H_2 could not be fully recovered when compared to the linear trend of the base response in 48.5% H_2 (H_2S-free), shown by the dotted line in Fig. 6(c). However, the cell exposed to 1 ppm H_2S in 97% H_2 was able to fully recover when run H_2S-free.

Considering the change in the HF intercept with time for the 9.7% H_2 case, it is seen that the ohmic resistance of the cell shows a very significant increase with time in the regime of H_2S exposure, as well as subsequent to its cessation.

To see how the HF and LF components contribute to the total polarization arc, each component is plotted separately as shown in Fig. 7. It is seen that the LF feature for the half cell exposed to 1 ppm H_2S in 97 and 48.5% H_2 (constant 3% H_2O) remains unchanged in the H_2S atmosphere and the total degradation was caused by the increase in the HF feature. The cell exposed to a low pH_2 (9.7% H_2, 3% H_2O) showed different behavior. It was observed that both the HF and LF were affected by exposure to H_2S and that this trend continued after cessation.

Considering the HF feature, it is seen that a two stage ('rapid' and 'slow') degradation profile is observed for the low pH_2 case (9.7% H_2), as observed for the higher hydrogen concentrations. However, at low pH_2 the LF feature did not remain constant but began to degrade after 7 h of H_2S exposure—leading to the observed constant increase in the total performance loss. After the removal of sulphur,
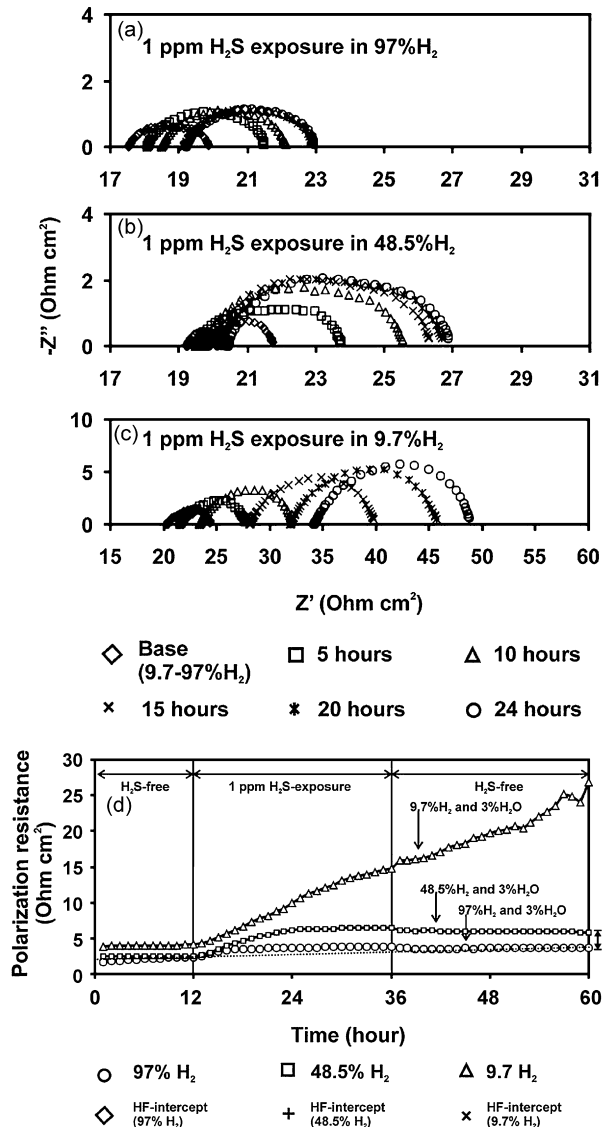

Fig. 6. EIS response of Ni–CGO half cell (Ni–CGO/YSZ/Ni–CGO) exposed to 1 ppm H_2S in varied H_2 concentrations: (a) 97% H_2; (b) 48.5% H_2; (c) 9.7% H_2, all at constant H_2S, H_2O content and temperature (1 ppm H_2S, 3% H_2O and 873 K); (d) polarization resistance obtained from equivalent circuit fitting. The dotted line indicates the linear trend extrapolated from the H_2S-free background for the impedance response in 48.5% H_2—showing partial recovery of the cell exposed to H_2S in 48.5% H_2.

both features continued increasing at nearly the same rate as in the course of sulphur (HF: 0.44 Ω cm^2 h^{-1} and LF: 0.27 Ω cm^2 h^{-1}). It was suspected that the bulk surface sulphide may begin to form and this can cause the unrecoverable performance.

This result suggests that lowering the H_2 content in the fuel mixture strongly enhances the interaction of sulphur with the anode, leading to greater performance degradation.

3.1.4. Effect of temperature on the interaction between H₂S and Ni–CGO anodes

The effect of temperature was studied on symmetrical cells exposed to 1 ppm H_2S. The gas mixture was maintained at a composition of 97% H_2/3% H_2O, while the operating temperature was measured at 873 K and 830 K on two separate cells. Fig. 8(a) and (b) shows that the impedance response was affected by the addition of H_2S at the two temperatures. The rate of total polarization resistance degradation (in the 'rapid' degradation regime) increased
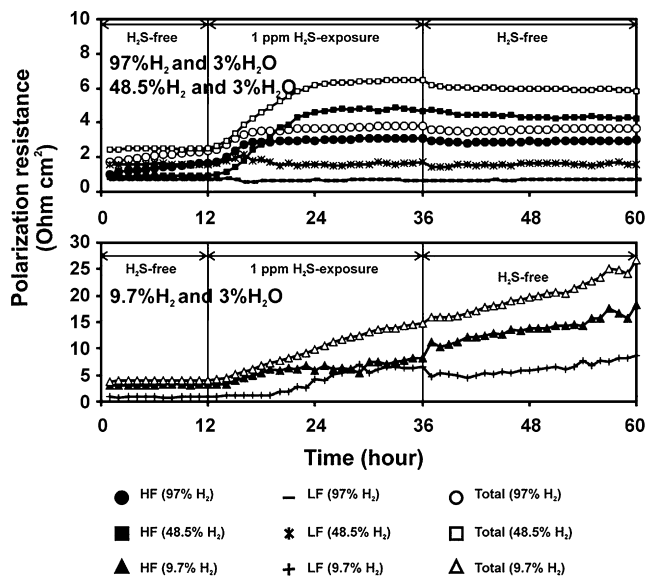
Fig. 7. High frequency, low frequency, and total EIS response when Ni–CGO half cells are exposed to 1 ppm H_2S in varied H_2 concentration: 97% H_2, 48.5% H_2, and 9.7% H_2 (1 ppm H_2S, 3% H_2O, 873 K).
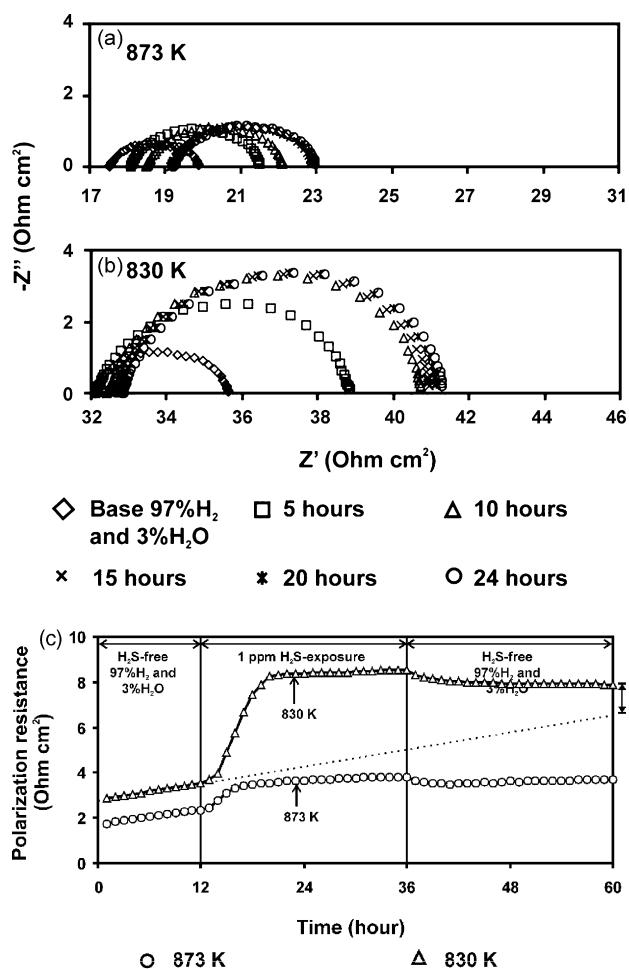

Fig. 8. EIS response of Ni–CGO half cell (Ni–CGO/YSZ/Ni–CGO) exposed to 1 ppm H_2S at varied temperature: (a) 873 K; (b) 830 K, both at constant H_2S, H_2 and H_2O content (1 ppm H_2S, 97% H_2, and 3% H_2O); (c) polarization resistance obtained from equivalent circuit fitting. The dotted line presents the linear trend extrapolated from the H_2S-free background for impedance response at 830 K—showing partial recovery of the cell exposed to H_2S at 830 K.
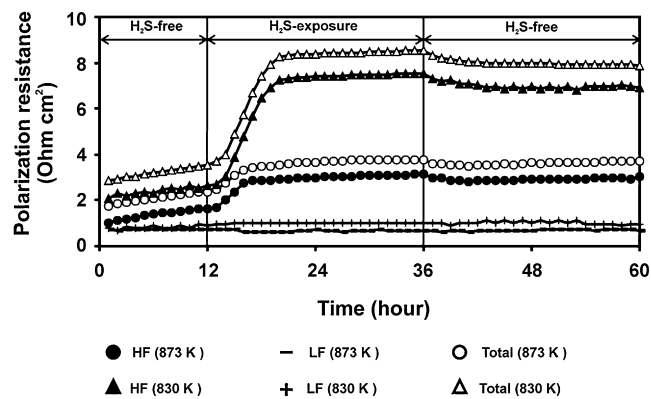

Fig. 9. High frequency, low frequency, and total EIS response when Ni–CGO half cells are exposed to 1 ppm H_2S in varied temperature: 830 and 873 K (97% H_2 and 3% H_2O).

from 0.26 to 0.72 $\Omega\,cm^2\,h^{-1}$ when the temperature was decreased from 873 to 830 K. The degree of performance loss ($\Delta R_{polarization}$) was found to increase from 1.4 to 4.8 $\Omega\,cm^2$ in going from 873 to 830 K, assuming a linear baseline. The HF-intercept remained unaffected by the addition of H_2S for both temperatures of operation.

Considering the plot in Fig. 9, it can be seen that in each case, the total increase in polarization resistance was primarily due to an increase in the HF feature associated with the resistance to charge transfer since there is no significant change in the LF feature due to sulphur introduction.

3.2. Comparison of electrochemical impedance results with thermodynamic calculations

Thermodynamic calculations have been made to predict the effect of gas composition (pH_2S and pH_2) and temperature on the interaction of H_2S with Ni and ceria. It should be stressed that phase predictions inherently relate to the bulk species and not the processes occurring at the surface. However, the trends that the thermodynamic calculations indicate, due to changes in the operating environment, can be reasonably associated with the trends that surface processes may follow, and as such are useful for making comparison with experimental results.

The calculations were performed using HSC Chemistry® 5.1 [35] to generate phase diagrams of the ternary component systems of Ni–O–S and Ce–O–S at 873 and 833 K. In order the compare the effect on Ni and ceria under the same conditions, the phase diagrams of Ni–O–S and Ce–O–S were combined on the same scale for each temperature, as shown in Fig. 10(a) and (b). The pO_2 value was calculated using the correlation between the partial pressure of species and the equilibrium constant of the reaction: $2H_2 + O_2 \rightarrow 2H_2O$. The pS_2 was calculated using the equilibrium constant for the two main reactions: $2H_2S + O_2 \rightarrow S_2 + 2H_2O$, and $2H_2S \rightarrow 2H_2 + S_2$. More details of this calculation and thermodynamic analysis applied to this system can be found in our previous work [36].

The points of operation indicated by the different symbols show that bulk sulphide is not expected to form for either the Ni or ceria. At an operating temperature of 873 K, Ni_3S_2 is the most thermodynamically stable phase at H_2S concentrations higher than ~1000 ppm (at 1000 ppm H_2S, 97% H_2, and 3% H_2O, $pO_2 = 10^{-27}$ and $pS_2 = 10^{-12}$ bar).

However, taking the movement of the operating points relative to the phase interface (i.e. indicator of the full and empty squares), it is found that the trends predicted by the bulk thermodynamic calculations and the EIS performance measurements
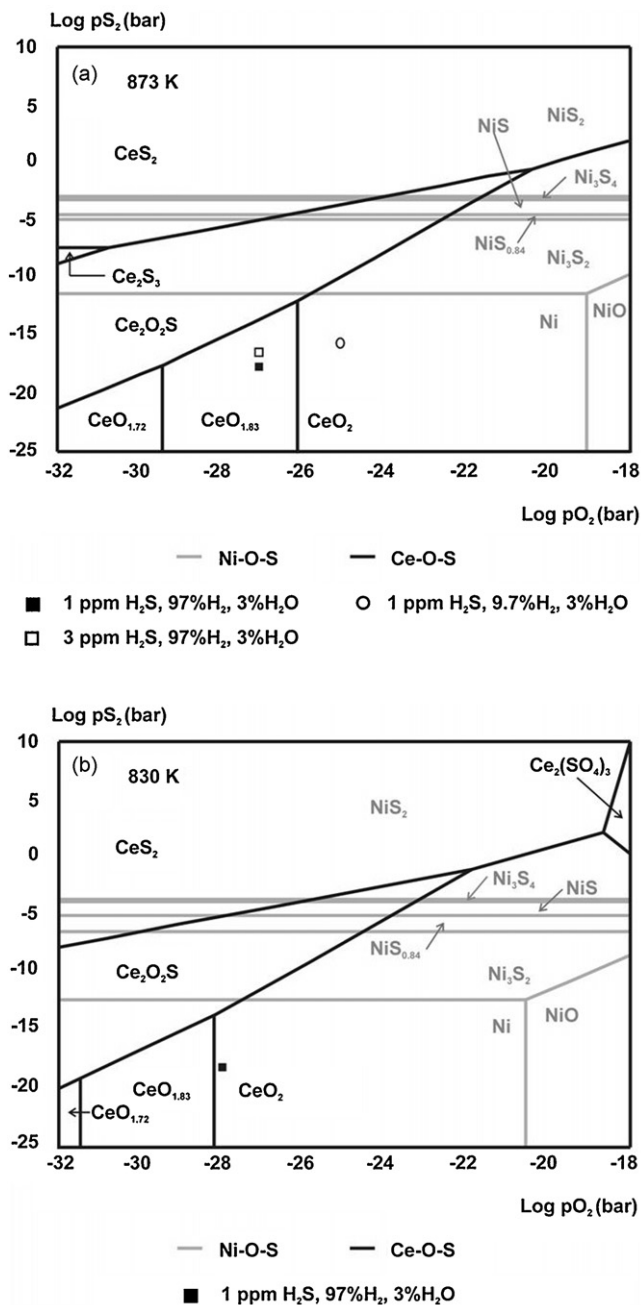
Fig. 10. Combined phase equilibrium of the Ni–O–S and Ce–O–S system at: (a) 873 K; (b) 830 K. The markers show the phase of Ni and ceria at different conditions: full square shows the conditions of 1 ppm H_2S in 97% H_2 and 3% H_2O; the empty square shows the conditions of 3 ppm H_2S in 97% H_2 and 3% H_2O; the circle shows the conditions of 1 ppm H_2S in 9.7% H_2 and 3% H_2O.

correlate. Increasing the H_2S concentration from 1 to 3 ppm shifts the pS_2 and moves to point vertically upwards, closer to the interface where Ni and ceria form a sulphide. Although not predicting a phase change, the movement relative to the phase boundary mirrors the trend for the H_2S to have an increasing impact on the anode as manifest through the EIS measurements.

The decreased H_2 content (from 97 to 9.7% H_2 at constant 3% H_2O, balance N_2) raises the pS_2 level—such that the reaction of sulphur with Ni is enhanced. Decreasing pH_2 also increases pO_2—causing ceria to turn from the sub-stoichiometric $CeO_{1.83}$ into stoichiometric CeO_2. The marker moves up-right (from the full

square to the circle). This reduces the propensity of sulphur to interact with ceria to form a sulphide, which is favourable when ceria is non-stoichiometric [36]. Therefore, the large increase of impedance response observed for the low pH_2 condition is likely to be due to the Ni component of the Ni–CGO anode.

Fig. 10(b) shows that decreasing the temperature from 873 to 830 K moves the equilibrium position for ceria to the stoichiometric form, but the effect of sulphur at such different temperatures cannot be seen clearly, compared to Fig 10(a). However, the previous work, with a larger temperature change (873–673 K), shows that as temperature decreases, the tendency of Ni to react with sulphur increases, although decreasing temperature actually lowers the pS_2 level [36]. This links with a large increase in impedance response when temperature decreased.

4. Conclusions

The impact of different operating conditions (pH_2S, pH_2 and temperature) on the interaction of H_2S with Ni–CGO anodes has been studied using electrochemical impedance spectroscopy, supported by thermodynamic calculations. EIS measurement shows that the extent of performance degradation worsens when pH_2S increases and pH_2 and temperature decrease. Consideration of the HF and LF component of the EIS response shows that performance loss is predominantly due to increase in the resistance to charge transfer. However, at higher pH_2S and lower pH_2, both HF and LF components are affected—indicating the effect of sulphur on both charge transfer and mass transport.

At low pH_2, cell performance degradation is irreversible and continues to degrade as nearly the same rate as when H_2S present. This contrasts to other cases, where the degraded performance is partially or fully recovered.

Thermodynamic calculations were compared to the EIS results. The calculations show that the tendency of the interaction of sulphur with the anode materials depends on the operating conditions, showing the dependency of the Ni–H_2S interaction on pS_2 and temperature as well as the ceria–H_2S interaction on pO_2 and pS_2. Increasing pH_2S raises the pS_2, enhancing the interaction of sulphur with both Ni and ceria. Electrochemical impedance shows a significant effect of H_2S concentration on both the rate and degree of anode performance degradation. Decreasing the pH_2 increases both pS_2 and pO_2—enhancing the interaction of sulphur with Ni but mitigating that with ceria, since the interaction of sulphur with stoichiometric ceria is lower [36–38]. Electrochemical measurement shows a fall in anode performance with decreasing pH_2—implying that the anode performance loss at low pH_2 is dominated by the interaction of sulphur with nickel rather than ceria. This is supported by thermodynamic prediction which shows a tendency for increased sulphur interaction with Ni at lower temperature.

The results of this study show that the gas composition and temperature have a significant impact on the interaction of sulphur with the anode. In a practical operating SOFC, different parts of the anode will be expected to degrade due to exposure to H_2S at different rates and extents depending on the local conditions. For example, as hydrogen is consumed within a fuel cell the pH_2 is lowered and therefore a greater degree of anode degradation towards the exit of the cell would be expected.

References

[1] W. Vielstich, A. Hubert, Handbook of Fuel Cells—Fundamentals, Technology and Applications, John Wiley & Sons, New York, 2003, p. 178.
[2] J. Larminie, A. Dicks, Fuel Cell System Explained, John Wiley & Sons, New York, 2002, p. 186.
[3] P.J. de Wild, R.G. Nyqvist, F.A. de Bruijn, E.R. Stobbe, J. Power Sources 159 (2006) 995.

[4] G.A. Richards, D.A. Berry, A. Freed, J. Power Sources 134 (2004) 49.

[5] M. Breysse, G. Djega-Mariadassou, S. Pessayre, G. Geantet, M. Vrinat, G. Pérot, M. Lemaire, Catal. Today 84 (2003) 129.

[6] X. Ma, S. Velu, J.H. Kim, C. Song, Appl. Catal. B: Environ. 56 (2004) 137.

[7] Y.H. Huang, R.I. Dass, Z.L. Xing, J.B. Goodenough, Science 312 (2006) 254.

[8] R. Mukundan, E.L. Brosha, F.H. Garzon, Electrochem. Solid State Lett. 7 (2004) A5.

[9] S. Tao, J.T.S. Irvine, Nat. Mater. 2 (2003) 320.

[10] J.W. Fergus, Solid State Ionics 177 (2006) 1529.

[11] S. Zha, P. Tsang, Z. Cheng, M. Liu, Solid State Chem. 178 (2005) 1844.

[12] L. Aguilar, S. Zha, S. Li, J. Winnick, M. Liu, Electrochem. Solid State Lett. 7 (2004) A324.

[13] Z. Cheng, S. Zha, L. Aguilar, M. Liu, Solid State Ionics 176 (2005) 1921.

[14] C. Yates, Y. Winnick, J. Electrochem. Soc. 146 (1999) 2841.

[15] D.R. Peterson, J. Winnick, J. Electrochem. Soc. 143 (1996) L55.

[16] H. He, R.J. Gorte, J.M. Vohs, Electrochem. Solid State Lett. 8 (2005) A279.

[17] A. Tomita, K. Tsunekawa, T. Hibino, S. Teranishi, Y. Tachi, M. Sano, Solid State Ionics 177 (2006) 2951.

[18] G.L. Wei, J.L. Luo, A.R. Sanger, K.T. Chuang, J. Electrochem. Soc. 151 (2004) A232.

[19] L. Aguilar, S. Zha, Z. Cheng, J. Winnick, M. Liu, J. Power Sources 135 (2004) 17.

[20] N.U. Pujare, K.W. Semkow, A.F. Sammells, J. Electrochem. Soc. 134 (1987) 2639.

[21] M. Liu, G.L. Wei, J.L. Luo, A.R. Sanger, K.T. Chuang, J. Electrochem. Soc. 150 (2003) A1025.

[22] G. Wei, M. Liu, J.L. Luo, A.R. Sanger, K.T. Chuang, J. Electrochem. Soc. 150 (2003) A463.

[23] Y. Matsuzaki, I. Yasud, Solid State Ionics 132 (2000) 261.

[24] S. Zha, Z. Cheng, M. Liu, J. Electrochem. Soc. 154 (2007) B201.

[25] M. Gong, X. Liu, J. Trembly, C. Johnson, J. Power Sources 168 (2007) 289.

[26] N.Q. Minh, T. Takahashi, Science and Technology of Ceramic Fuel Cells, Elservier Science, New York, 1995, p. 154.

[27] J. Dong, Z. Cheng, S. Zha, M. Liu, J. Power Sources 156 (2006) 461.

[28] S.A. Baron, N.P. Brandon, A. Atkinson, B.H.C. Steele, R. Rudkin, J. Power Sources 126 (2004) 58.

[29] B.A. Boukamp, Solid State Ionics 20 (1986) 31.

[30] G.J. Brug, A.L.G. van den Eeden, M. Sluyters-Rehbach, J.H. Sluyters, J. Electroanal. Chem. 176 (1984) 275.

[31] J.B. Jorcin, M.E. Orazem, N. Pébère, B. Tribollet, Electrochim. Acta 51 (2006) 1473.

[32] K. Sasaki, K. Susuki, A. Iyoshi, M. Uchimura, N. Imamura, H. Kusaba, Y. Teraoka, H. Fuchino, K. Tsujimoto, Y. Uchida, N. Jingo, J. Electrochem. Soc. 153 (2006) A2023.

[33] S. Mukerjee, K. Haltiner, R. Kerr, L. Chick, V. Sprenkle, K. Meinhardt, C. Lu, J.Y. Kim, K.S. Weil, Proceedings of the 10th International Symposium on Solid Oxide Fuel Cells (SOFC-X), Nara, Japan, 2007, p. 59.

[34] A. Ishikura, S. Sakuno, N. Komiyama, H. Sasatsu, N. Masuyama, H. Itoh, K. Yasumoto, Proceedings of the 10th International Symposium on Solid Oxide Fuel Cells (SOFC-X), Nara, Japan, 2007, p. 845.

[35] OUTOKUMPU, HSC Chemistry for Windows, Version 5.1.

[36] P. Lohsoontorn, D.J.L. Brett, N.P. Brandon, J. Power Sources 175 (2007) 60.

[37] Y. Zeng, S. Kaytakoglu, D.P. Harrison, Chem. Eng. Sci. 55 (2000) 4893.

[38] Y. Zeng, S. Zhang, F.R. Groves, D.P. Harrison, Chem. Eng. Sci. 154 (1999) 3007.